CHINESE OPTICS LETTERS

Vol. 21, No. 11 | November 2023

Polarization and magneto-optical characteristics of Tb:YAG crystal-derived silica fiber via laser-heating drawing technique

Hao Shi (时 昊), Jianxiang Wen (文建湘)*, Beibei Xing (邢蓓蓓), Yanhua Luo (罗艳华), Xiaobei Zhang (张小贝), Fufei Pang (庞拂飞), and Tingyun Wang (王廷云)

Key Laboratory of Specialty Fiber Optics and Optical Access Networks, Joint International Research Laboratory of Specialty Fiber Optics and Advanced Communication, School of Communication and Information Engineering, Shanghai University, Shanghai 200444, China

*Corresponding author: wenjx@shu.edu.com

Received June 15, 2023 | Accepted July 6, 2023 | Posted Online November 5, 2023

Fiber quarter-wave plates and magneto-optical fibers are important components that greatly affect the sensitivity of fiber-optic current sensors. A Tb:YAG crystal-derived silica fiber (TYDSF) was fabricated using a CO_2 laser-heating drawing technique. The linear birefringence of TYDSF was measured as 6.661×10^{-6} by a microscope birefringence measurement instrument. A fiber quarter-wave plate was fabricated by TYDSF at 1310 nm, which produced circularly polarized light with a polarization extinction ratio of 0.34 dB. Additionally, the linear birefringence of TYDSF was decreased by 22% by annealing at 750°C for 7 h, and the Verdet constants of annealed TYDSF were measured to be 9.83, 6.67, and 3.48 rad/(T · m) at 808, 980, and 1310 nm, respectively.

Keywords: Faraday effect; linear birefringence; fiber quarter-wave plate.
DOI: 10.3788/COL202321.110601

1. Introduction

Fiber-optic current sensors (FOCSs) based on the Faraday effect have promising development prospects in the field of high current transmission and measurement. Compared to traditional current sensors, FOCS has great advantages because of its smaller size, resistance to electromagnetic interference, and no saturation effects[1–3]. A fiber quarter-wave plate is capable of transforming linearly polarized light into circularly polarized light, as well as circularly polarized light into linearly polarized light, whose quality directly affects the precision of FOCS. Fiber quarter-wave plates are mainly composed of highly birefringent fibers[4,5] with a beat length in the millimeter range, which requires precise length control. The polarization-transforming fiber could also be used as a quarter-wave plate[6,7], which is not sensitive to temperature changes. However, the fabrication process of the variable rate spun fiber is complicated, making this solution not universally applicable.

The standard silica fibers (SFs) that are commonly used as magneto-optical fibers in FOCS exhibit a weak Faraday effect. This weakness leads to a significant increase in fiber length, resulting in a reduction in the sensitivity of the FOCS due to the linear birefringence. A spun highly birefringent fiber is a promising candidate for FOCS[8]. An alternate approach to achieving high-sensitivity FOCS is to increase the Faraday effect of the fiber through doping ions with strong magneto-optical properties into optical fibers, so that the length of the magneto-optical fiber required for FOCS is shorter. Multicomponent glass fibers could achieve high Verdet constants[9–11]. In particular, Ref. [12] has reported a 56% (mass fraction) terbium-doped fiber with a Verdet constant of -24.5 ± 1.0 rad/(T · m) at 1053 nm, which is 20 times greater than that of the standard SF. However, the compatibility of the glass fiber with standard SFs is poor, making it difficult to integrate them into FOCS. SFs doped with fewer rare-earth ions have significant advantages, such as smaller thermal expansion coefficients and lower transmission loss[13–17]. However, these types of fibers are subject to concentration quenching, limiting the doping concentration and resulting in a low Verdet constant.

YAG crystal-derived silica fibers (YDSFs), which are made with yttrium aluminosilicate glass cores, have offered several advantages over other multicomponent glass core fibers, including superior physical and chemical stability, and excellent compatibility with standard SFs[18–20]. Moreover, YDSFs can accommodate significantly higher concentrations of ions than conventional doped SFs. Tb^{3+} ions have a strong Faraday effect because of the electronic transition of $4f^n \rightarrow 4f^{n-1}5d$. Additionally, Tb^{3+} ions demonstrate good transparency in the visible to near infrared range.

In this work, we fabricated a Tb:YAG crystal-derived silica fiber (TYDSF) with high Tb^{3+} concentration based on a CO_2 laser-heating drawing technique. The linear birefringence of TYDSF was measured through a microscope birefringence measurement instrument, and a fiber quarter-wave plate was fabricated by TYDSF. Additionally, the TYDSF was annealed to reduce linear birefringence, and the Verdet constant of TYDSF was measured.

2. Experimental Procedure

2.1. Fiber fabrication and properties

A TYDSF was fabricated on a CO_2 laser-heating drawing tower using the molten-core method[21]. Compared to conventional graphite heating, CO_2 laser heating provides several advantages, such as smaller high-temperature zones, faster heating speeds, and better parameter control, resulting in reduced cladding diffusion[22]. The melting point of TYDSF is approximately 1900°C; its cladding is composed of highly pure SiO_2. Therefore, TYDSF exhibits good compatibility with standard SF. The element concentrations of O, Si, Y, Al, and Tb in TYDSF, which are measured by an electron probe microanalyzer (C10633, Hamamatsu, Japan) are 45.54%, 17.15%, 16.48%, 10.67%, and 10.15% (mass fractions), respectively. Figure 1(a) shows the refractive index distribution of TYDSF using a fiber refractive index analyzer (S14, Photon Kinetics Inc., U.S.). As a result of high concentration doping materials in the fiber core, the relative refractive index difference and numerical aperture were calculated to be 1.5% and 0.25, respectively. The TYDSF features a uniform core and cladding, with measurements of 5.6 and 125.8 μm, respectively. The attenuation characteristics of TYDSF depicted in Fig. 1(b) were determined using the cut-back method with an optical spectrum analyzer (OSA, AQ6315, Yokogawa, Japan). It is evident that TYDSF exhibits exceptional transmission capabilities, ranging from 600 to 1500 nm.

The excitation and emission spectra of TYDSF shown in Fig. 1(c) were measured using a fluorescence spectrophotometer (Edinburgh FLS-980, UK). The four emission peaks at 487, 543, 586, and 620 nm are excited at 241 nm. The energy level transitions of four emission peaks are $^5D_4 \rightarrow {}^7F_6$, $^5D_4 \rightarrow {}^7F_5$, $^5D_4 \rightarrow {}^7F_4$, and $^5D_4 \rightarrow {}^7F_3$, respectively[23].

2.2. Heat treatment and birefringence measurement methods

To eliminate the stress generated during the fiber drawing process that could increase the linear birefringence, TYDSF was annealed at 350°C, 450°C, 550°C, 650°C, 750°C, 850°C, and 950°C for 7 h, respectively. The heat treatment was carried out in a muffle (SXL-1700C, China), whose highest heating rate and highest heating temperature were 10°C/min and 1700°C, respectively. The sample of TYDSF was put on the edge of the ceramic cup to prevent the cross section of the fiber from being contaminated or damaged, and then the ceramic cup was placed into the muffle, as shown in Fig. 2(a). Subsequently, we used a microscope birefringence measurement instrument (MicroImager, Hinds Instruments, U.S.) to determine the annealing temperature at which the linear birefringence of TYDSF could be eliminated to the greatest extent, as shown in Fig. 2(b). Ref. [24] explains the basic structure and principles of this instrument. Compared to other methods, which need to construct an entire system[25,26], it can measure the linear birefringence of samples faster and more efficiently. The spatial digital resolution of this instrument is 0.7 μm, and the detection limit (background noise) for retardance is 0.1 nm. The measurement range for retardance is from 0.1 to 3500 nm.

We adhered seven samples, which had been annealed at different temperatures, as well as an unannealed sample onto the side of a glass slide, as depicted in Fig. 2(c). The samples were then placed on the sample stage of the microscope birefringence measurement instrument. By adjusting the X–Y and focus controller of the sample stage, the cross section of the fiber samples was clearly observed. Subsequently, the retardance and intensity distribution of these fiber samples were obtained

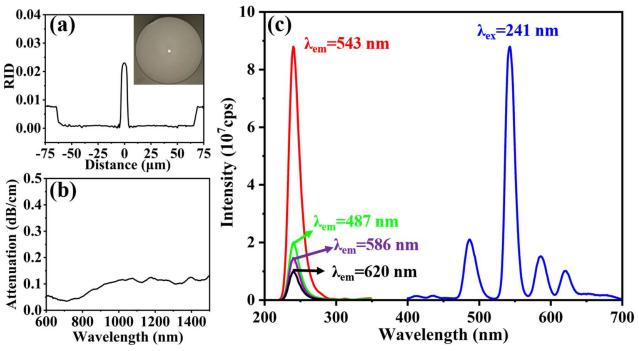

Fig. 1. Basic optical characteristics of TYDSF. (a) Refractive index distribution (RID) of TYDSF (the inset is the profile of the TYDSF observed under a microscope). (b) Attenuation spectrum of TYDSF. (c) Excitation and emission spectra of TYDSF.

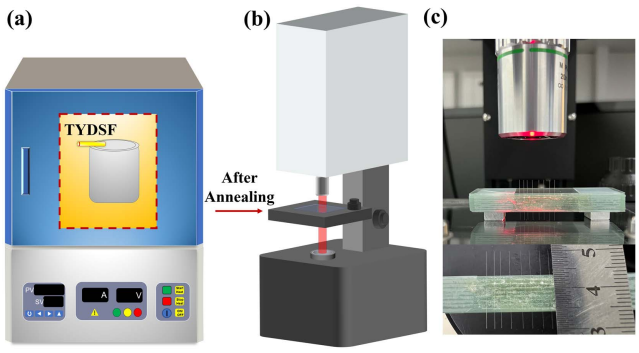

Fig. 2. Schematic diagram of the annealing process and the linear birefringence measurement of TYDSF. (a) Schematic diagram of TYDSF annealing. (b) Schematic diagram of microscope birefringence measurement instrument. (c) Picture of TYDSF samples for linear birefringence measurement.

through the software of the microscope birefringence measurement instrument.

2.3. State of polarization and Faraday rotation measurements of TYDSF

To ensure accurate measurement of the state of polarization and Verdet constants of fiber samples, a system has been set up, as depicted in Fig. 3. The system comprises four main parts: the laser, a polarization control section, a magnetic field, and a Stokes polarimeter. The polarization control section includes one collimating lens (L), two polarizers (P_1 and P_2), one quarter-wave plate (Q), and one objective (O). After passing through Q, the state of polarization of light changes from linear polarization to circular polarization. By rotating P_2, the linearly polarized light can be coupled into the fiber from different angles while ensuring that the power of light is almost the same. The WD-50 electromagnetic coil is used as the magnetic field, with an adjustable air gap range of 0 to 80 mm. By using a Stokes polarimeter (PAX5710, Thorlabs, U.S.), the state of polarization of output light can be determined, and Faraday rotation can be measured by activating the electromagnet.

In the experiment, the core diameter of the input fiber (HI-1060) is matched with that of the TYDSF, thereby avoiding offset excitation of high-order modes. Additionally, fiber samples are relatively short and kept in a completely relaxed state, which is not easy to excite in high-order modes. Furthermore, we detect the mode patterns before and after the TYDSF (positions "A" and "B") in order to ensure that the fundamental mode propagation in the fiber samples mainly exists there. The Faraday effect is a magneto-optical phenomenon[27] that occurs when the plane of linearly polarized light rotates at a certain angle and the light propagates through a magneto-optically active material. The rotation of polarization plane θ can be expressed as[28]

$$\theta = V \cdot B_m \cdot L, \tag{1}$$

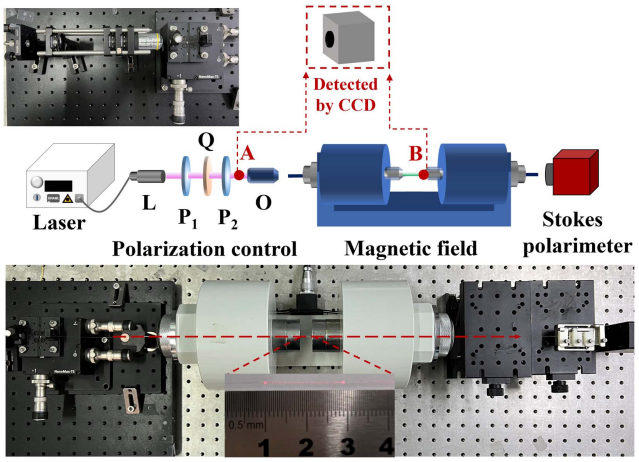

Fig. 3. Measurement system of state of polarization and Faraday rotation for optical fibers.

where B_m is the longitudinal component of the magnetic field strength, and L is the length of magnetic field. V is the Verdet constant, which represents the strength of the Faraday effect of magneto-optical materials.

2.4. Theory of birefringence in fibers

The transmission Jones matrix of TYDSF under the influence of linear birefringence could be equivalent to a linear retarder[29], whose fast axis is parallel to the x axis given by

$$M_\delta = \begin{bmatrix} e^{-j(\frac{\delta}{2})} & 0 \\ 0 & e^{j(\frac{\delta}{2})} \end{bmatrix}. \tag{2}$$

In Eq. (2), δ is phase retardance and is given by $\delta = 2\pi BL/\lambda$, where B is linear birefringence, L is the length of fiber, and λ is wavelength. To perform as a quarter-wave plate, a segment of the fiber should have a length of

$$L_{\frac{1}{4}\lambda} = \frac{\lambda\left(\frac{1}{4} + \frac{n}{2}\right)}{B}, \tag{3}$$

where n is a nonnegative integer. In the system shown in Fig. 3, linearly polarized light can be incident into the fiber at any angle. Therefore, the state of polarization of the output light could be expressed as

$$E_{\text{out}} = M_\delta \cdot E_{\text{in}} = \begin{bmatrix} e^{-j(\frac{\delta}{2})} & 0 \\ 0 & e^{j(\frac{\delta}{2})} \end{bmatrix} \cdot \begin{bmatrix} \cos\theta \\ \sin\theta \end{bmatrix} = e^{-j(\frac{\delta}{2})} \begin{bmatrix} \cos\theta \\ e^{j\delta}\sin\theta \end{bmatrix}, \tag{4}$$

where E_{in} is the state of polarization of the input light and θ is the angle between the linearly polarized light and the x axis. Subsequently, we can calculate the azimuth φ and ellipticity χ of E_{out} given by

$$\tan 2\varphi = \tan 2\theta \cos\delta, \tag{5a}$$

$$\sin 2\chi = \sin 2\theta \sin\delta. \tag{5b}$$

By substituting Eq. (3) into Eqs. (5a) and (5b), the state of polarization of the output light from the fiber quarter-wave plate can be obtained.

The Faraday effect is a kind of circular birefringence. Therefore, in the presence of a magnetic field, elliptical birefringence occurs, so the state of polarization of output light can be expressed as[30]

$$\begin{aligned} E'_{\text{out}} &= M_\phi \cdot E_{\text{in}} \\ &= \begin{bmatrix} \cos\frac{\phi L}{2} - j\frac{\Delta\beta}{\phi}\sin\frac{\phi L}{2} & -\frac{2F}{\phi}\sin\frac{\phi L}{2} \\ \frac{2F}{\phi}\sin\frac{\phi L}{2} & \cos\frac{\phi L}{2} + j\frac{\Delta\beta}{\phi}\sin\frac{\phi L}{2} \end{bmatrix} \cdot \begin{bmatrix} \cos\theta \\ \sin\theta \end{bmatrix} \\ &= \begin{bmatrix} A + jB \\ C + jD \end{bmatrix}, \end{aligned} \tag{6}$$

where M_ϕ is the transmission matrix of elliptical birefringence. F is the Faraday rotation per unit length, $\Delta\beta$ is the phase retardance per unit length given by $\Delta\beta = 2\pi B/\lambda$, and ϕ is given by $\phi^2 = (2F)^2 + \Delta\beta^2$. To simplify the complexity of subsequent equations, Eq. (6) is simplified through letters. The azimuth of the E'_{out} can be represented as[29]

$$\tan 2\varphi' = \frac{2(AC + BD)}{A^2 + B^2 - C^2 - D^2} = f(\theta, F). \tag{7}$$

Combined with Eq. (5a), the relationship between the Faraday rotation $\Delta\varphi = (\varphi' - \varphi)$ and the input azimuth θ can be expressed as

$$f(\theta, F) = \tan\left\{2\Delta\varphi + \arctan\left[\tan 2\theta \cdot \cos\left(\frac{2\pi BL}{\lambda}\right)\right]\right\}. \tag{8}$$

3. Experimental Results and Discussion

3.1. Linear birefringence of annealed TYDSF

As shown in the insets on the left in Figs. 4(a)–4(h), the magnitude of the retardance is calibrated by the color map, and it is obvious that the retardance of the fiber core is high. In the supporting software, the retardance data can be plotted using four straight lines passing through the center of the fiber core, as shown by the retardance curves in Fig. 4. The length of these samples is 2 cm, and their linear birefringence B can be calculated by $B = \Delta n/L$, as shown in Table 1, where Δn is the average of the highest values of the four retardance curves. As TYDSF is annealed at a temperature of 750°C, its linear birefringence is significantly reduced to the greatest extent, resulting in a decrease of 22%. Once the temperature exceeds 750°C, the linear birefringence of TYDSF increases instead of decreasing. This phenomenon may be attributed to the presence of ions within the fiber, which undergo alterations beyond a certain temperature threshold[31].

3.2. Polarization characteristic of TYDSF

According to Eq. (3), a fiber quarter-wave plate can be made by unannealed TYDSF at 1310 nm when $L = 4.92$ cm.

When the angle between the linearly polarized light and the fast axis of the fiber quarter-wave plate is ±45°, right-handed and left-handed circularly polarized light can be formed, as shown in Fig. 5(b), with ellipticity of 44° and −44.3°. The polarization extinction ratio of the right-handed and left-handed circularly polarized light was measured to be 0.38 and 0.34 dB, respectively, which belonged to high-quality circularly polarized light. It seems that TYDSF is well suited for making high-quality quarter-wave plates because the impact of interception length errors can be reduced when the beat length of the fiber is in the centimeter range.

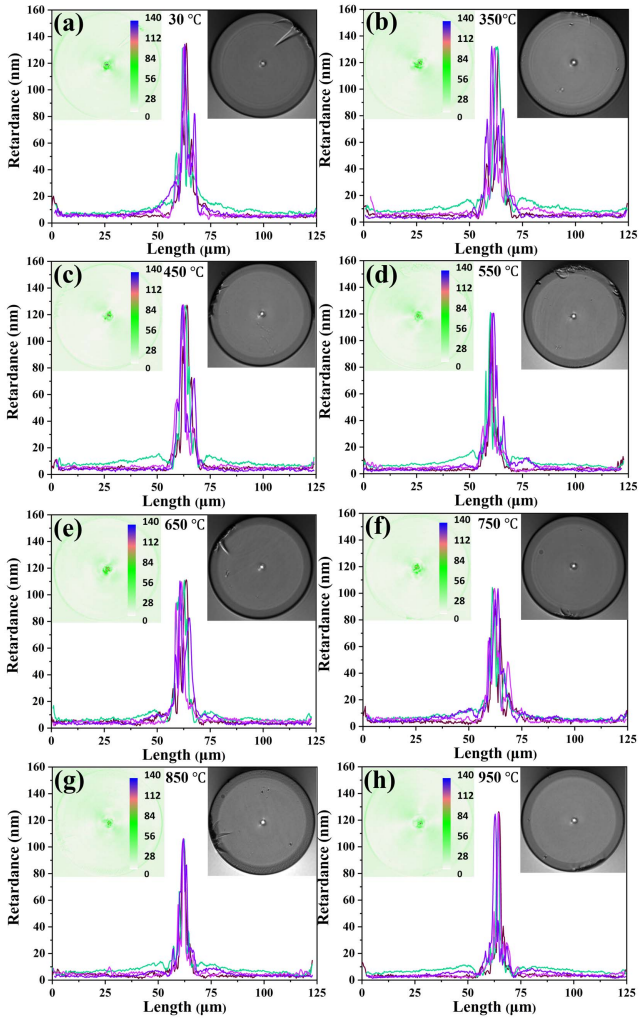

Fig. 4. Retardance curves in four directions of TYDSF samples (a) without annealing and annealed at (b) 350°C, (c) 450°C, (d) 550°C, (e) 650°C, (f) 750°C, (g) 850°C, (h) 950°C (the insets on the left are the retardance distributions and color maps. The insets on the right are the intensity distributions).

Table 1. Linear Birefringence of TYDSF after Annealing at Different Temperatures.

Annealing Temperature	B (10^{-6})
Without annealing	6.6610
350°C	6.5641
450°C	6.3579
550°C	6.0246
650°C	5.5270
750°C	5.1813
850°C	5.2844
950°C	6.2614

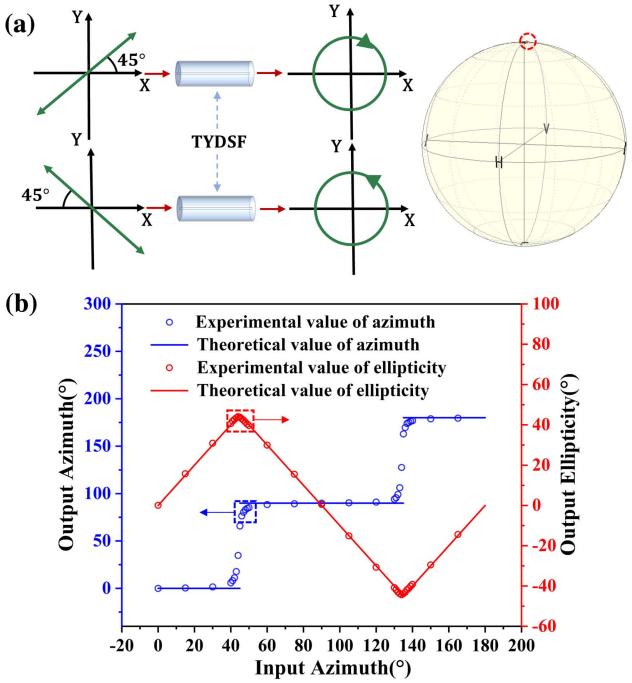

Fig. 5. Output polarization state of TYDSF with the length of a quarter beat length. (a) Schematic diagram of the transformation of linearly polarized light into right-handed and left-handed circularly polarized light in a fiber quarter-wave plate; (b) evolution of azimuth and ellipticity of the output state of polarization versus the input azimuth in a fiber quarter-wave plate.

3.3. Faraday effect of TYDSF

As the fiber length exceeds half of the beat length, the Faraday rotation is significantly reduced, due to the linear birefringence existing in the fiber samples[30]. Additionally, when the polarization state of the output light is almost circular polarization, the experimental value of output azimuth is more susceptible to errors, as shown in Fig. 5(b). Therefore, the length of TYDSF in the experiment should be less than a quarter of the beat length. TYDSF with a length of 2 cm will be measured for Faraday rotation at 808, 980, and 1310 nm, respectively. According to the previous section, it can be concluded that the linear birefringence of TYDSF was reduced to the greatest extent after annealing at 750°C, so the measurement of Faraday rotation is conducted on unannealed TYDSF and TYDSF annealed at 750°C.

The experimental Faraday rotation $\Delta\varphi$ of TYDSF was measured at three different wavelengths before and after annealing, as shown in Figs. 6(b)–6(d), while Fig. 6(a) shows the experimental Faraday rotation of the standard SF. It is clear that the experimental Faraday rotation of TYDSF changes with the input azimuth θ due to the influence of linear birefringence, while the standard SF does not exhibit this phenomenon. According to Eq. (8), $F \cdot L$ can be calculated. In theory, $F \cdot L$ is the intrinsic Faraday rotation of the fiber and has the same value at different input azimuths. However, the experimental Faraday rotation $\Delta\varphi$ is affected by experimental errors, so the calculated $F \cdot L$ can be considered as a compensated value. Although $F \cdot L$ calculated

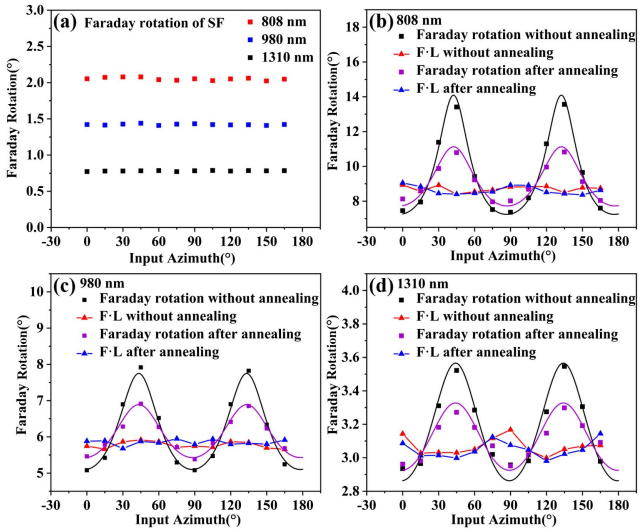

Fig. 6. Faraday rotation of fiber samples. (a) Faraday rotation of SF at 808, 980, and 1310 nm; Faraday rotation and compensated value ($F \cdot L$) of TYDSF at (b) 808 nm, (c) 980 nm, and (d) 1310 nm.

for each input azimuth is not consistent, the amplitude of its fluctuation is much smaller than experimental Faraday rotation. Furthermore, the experimental Faraday rotation of TYDSF is closer to $F \cdot L$ after annealing than that of unannealed TYDSF. The average values of $F \cdot L$ before and after annealing were then calculated at each wavelength, as shown in Table 2.

Subsequently, according to Eq. (8), the relationship between $\Delta\varphi$ and θ can be obtained, as shown by the solid line in Figs. 6(b)–6(d). It is worth noting that when the input azimuth is 45° and 135°, a relatively large Faraday rotation will be obtained, but this is not the maximum value, and theoretically the maximum value will be obtained when the input azimuth is slightly less than 45° and 135°. As shown in Table 2, the average $F \cdot L$ of TYDSF remains nearly the same before and after annealing, indicating that its intrinsic Faraday effect has not been altered. The average magnetic field, measured through a Gauss meter, is found to be 0.7656 T. Therefore, the Verdet constants of the annealed TYDSF can be calculated as 9.83, 6.67, and 3.48 rad/(T · m) at 808, 980, and 1310 nm, respectively, as shown in Fig. 7.

Table 2. Average $F \cdot L$ of TYDSF before and after Annealing at 808, 980, and 1310 nm.

	Average $F \cdot L$ (°)	
Wavelength (nm)	Without Annealing	Annealing at 750°C
808	8.710	8.627
980	5.775	5.848
1310	3.067	3.049

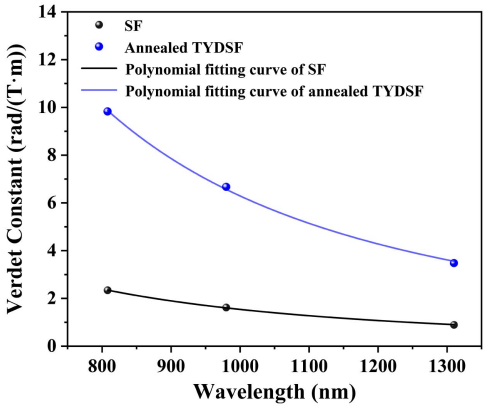

Fig. 7. Verdet constants of SF and TYDSF at 808, 980, and 1310 nm.

4. Conclusion

In this study, TYDSF was fabricated based on a CO_2 laser-heating drawing technique. The linear birefringence of TYDSF was measured using a microscope birefringence measurement instrument. A reliable system was constructed to measure the state of polarization and Faraday rotation of fibers. TYDSF was used to fabricate a fiber quarter-wave plate at 1310 nm, which produced circularly polarized light with an ellipticity of −44.3° and a polarization extinction ratio of 0.34 dB. Since the Faraday rotation could be affected by the linear birefringence, the TYDSF was annealed at 350°C, 450°C, 550°C, 650°C, 750°C, 850°C, and 950°C for 7 h to reduce the linear birefringence. Annealing TYDSF at 750°C can lead to a substantial reduction in linear birefringence, with a maximum reduction of 22%. It was found that the Faraday rotation of TYDSF after annealing had smaller fluctuations with different input azimuths than that of before annealing. Finally, based on the Jones matrix, the measured Faraday rotation was compensated, resulting in a value closer to the theoretical Faraday rotation of TYDSF. The Verdet constants of TYDSF at 808, 980, and 1310 nm were found to be 9.83, 6.67, and 3.48 rad/(T · m), respectively, which were 4.20, 4.12, and 3.91 times those of the standard SF. Therefore, it is evident that TYDSF is a good candidate for a fiber quarter-wave plate and a magneto-optical fiber, which is used in FOCSs, magneto-optical isolators, and magneto-optical modulators.

Acknowledgement

This work was supported by the National Natural Science Foundation of China (Nos. 61935002, 61975113, and 62275148), the 111 Project (No. D20031), the Shanghai Professional Technical Public Service Platform of Advanced Optical Waveguide Intelligent Manufacturing and Testing (No. 19DZ2294000), and the Jiangsu Province's Industry Outlook and Key Core Technologies–Key Projects (No. BE2022055-4).

References

1. V. Temkina, A. Medvedev, and A. Mayzel, "Research on the methods and algorithms improving the measurements precision and market competitive advantages of fiber optic current sensors," Sensors **20**, 5995 (2020).
2. K. Bohnert, C.-P. Hsu, L. Yang, A. Frank, G. M. Müller, and P. Gabus, "Fiber-optic current sensor tolerant to imperfections of polarization-maintaining fiber connectors," J. Light. Technol. **36**, 2161 (2018).
3. R. M. Silva, H. Martins, I. Nascimento, J. M. Baptista, A. L. Ribeiro, J. L. Santos, P. Jorge, and O. Frazão, "Optical current sensors for high power systems: a review," Appl. Sci. **2**, 602 (2012).
4. H. Gao, G. Wang, W. Gao, S. Li, Y. Wang, B. Zhao, and R. Zhang, "A method for suppressing error of fiber optic current transformer caused by temperature based on $\lambda/4$ wave plate fabricated with polarization maintaining photonic crystal fiber," IEEE Sens. J. **23**, 10517 (2023).
5. Z. Shi, M. Ji, J. Lin, M. Li, and Y. Bai, "Quarter wave plate made by cutting straight holey birefringent fiber," Proc. SPIE **7134**, 713449 (2008).
6. A. H. Rose, N. Feat, and S. M. Etzel, "Wavelength and temperature performance of polarization-transforming fiber," Appl. Opt. **42**, 6897 (2003).
7. N. Peng, Y. Huang, S. Wang, T. Wen, W. Liu, Q. Zuo, and L. Wang, "Fiber optic current sensor based on special spun highly birefringent fiber," IEEE Photon. Technol. Lett. **25**, 1668 (2013).
8. P. Yao, X. Chen, P. Hao, H. Xiao, Z. Ding, T. Liu, and X. S. Yao, "Introduction and measurement of the effective Verdet constant of spun optical fibers," Opt. Express **29**, 23315 (2021).
9. D. F. Franco, R. G. Fernandes, J. F. Felix, V. R. Mastelaro, H. Eckert, C. R. M. Afonso, Y. Messaddeq, S. H. Messaddeq, S. Morency, and M. Nalin, "Fundamental studies of magneto-optical borogermanate glasses and derived optical fibers containing Tb^{3+}," J. Mater. Res. Technol. **11**, 312 (2021).
10. K. Linganna, S. Ju, Y. Lee, and W.-T. Han, "Development of aluminosilicate glass fiber doped with high Pr^{3+} concentration for all-optical fiber isolator application," J. Mater. Sci. Mater. Electron. **30**, 12790 (2019).
11. Q. Chen, H. Wang, Q. Wang, and Q. Chen, "Faraday rotation influence factors in tellurite-based glass and fibers," Appl. Phys. A **120**, 1001 (2015).
12. L. Sun, S. Jiang, J. D. Zuegel, and J. R. Marciante, "All-fiber optical isolator based on Faraday rotation in highly terbium-doped fiber," Opt. Lett. **35**, 706 (2010).
13. Y. Huang, H. Chen, W. Dong, F. Pang, J. Wen, Z. Chen, and T. Wang, "Fabrication of europium-doped silica optical fiber with high Verdet constant," Opt. Express **24**, 18709 (2016).
14. L. Yang, J. X. Wen, Y. Wu, Y. Wan, L. Z. Zeng, W. Chen, F. F. Pang, X. B. Zhang, and T. Y. Wang, "High signal-to-noise ratio fiber laser at 1596 nm based on a Bi/Er/La co-doped silica fiber," Chin. Opt. Lett. **20**, 051402 (2022).
15. Y. G. Chen, Z. Q. Lin, Y. F. Wang, M. Wang, L. Zhang, Y. Jiao, H. H. Dong, S. K. Wang, C. L. Yu, and L. L. Hu, "Nd^{3+}-doped silica glass and fiber prepared by modified sol-gel method," Chin. Opt. Lett. **20**, 091601 (2022).
16. Q. Guo, J. Wen, Y. Huang, W. Wang, F. Pang, Z. Chen, Y. Luo, G.-D. Peng, and T. Wang, "Magneto-optical properties and measurement of the novel doping silica optical fibers," Measurement **127**, 63 (2018).
17. J. Wen, Q. Che, Y. Dong, Q. Guo, F. Pang, Z. Chen, and T. Wang, "Irradiation effect on the magneto-optical properties of Bi-doped silica optical fiber based on valence state change," Opt. Mater. Express **10**, 88 (2020).
18. S. Zheng, J. Li, C. Yu, Q. Zhou, and D. Chen, "Preparation and characterizations of Nd:YAG ceramic derived silica fibers drawn by post-feeding molten core approach," Opt. Express **24**, 24248 (2016).
19. G. Tang, G. Qian, W. Lin, W. Wang, Z. Shi, Y. Yang, N. Dai, Q. Qian, and Z. Yang, "Broadband 2 μm amplified spontaneous emission of Ho/Cr/Tm:YAG crystal derived all-glass fibers for mode-locked fiber laser applications," Opt. Lett. **44**, 3290 (2019).
20. Y. Wan, J. Wen, C. Jiang, F. Tang, J. Wen, S. Huang, F. Pang, and T. Wang, "Over 255 mW single-frequency fiber laser with high slope efficiency and power stability based on an ultrashort Yb-doped crystal-derived silica fiber," Photonics Res. **9**, 649 (2021).
21. J. Ballato and A. C. Peacock, "Perspective: molten core optical fiber fabrication—a route to new materials and applications," APL Photonics **3**, 120903 (2018).

22. X. Ji, S. Lei, S.-Y. Yu, H. Y. Cheng, W. Liu, N. Poilvert, Y. Xiong, I. Dabo, S. E. Mohney, J. V. Badding, and V. Gopalan, "Single-crystal silicon optical fiber by direct laser crystallization," ACS Photonics **4**, 85 (2017).
23. H. Yang and Z. Zhu, "Magneto-optical glass mixed with Tb^{3+} ions: high Verdet constant and luminescence properties," J. Lumin. **231**, 117804 (2021).
24. D. H. Goldstein, L. L. Deibler, and B. B. Wang, "Measurement of small birefringence in sapphire and quartz plates," Proc. SPIE **4819**, 20 (2002).
25. E. Kuzin, J. M. Estudillo-Ayala, B. Ibarra-Escamilla, and J. Haus, "Measurements of beat length in short low-birefringence fibers," Opt. Lett. **26**, 1134 (2001).
26. Y. Yang, W. Duan, and M. Ye, "High precision measurement technology for beat length of birefringence optical fiber," Meas. Sci. Technol. **24**, 025201 (2013).
27. V. F. Nezhad, C. L. You, and G. Veronis, "Nanoplasmonic magneto-optical isolator," Chin. Opt. Lett. **19**, 083602 (2021).
28. M. Basharat, M. Ding, Y. Li, H. W. Cai, and J. C. Fang, "Noise reduction and signal to noise ratio improvement in magneto-optical polarization rotation measurement," Chin. Opt. Lett. **16**, 081201 (2018).
29. T. Chartier, A. Hideur, C. Özkul, F. Sanchez, and G. M. Stéphan, "Measurement of the elliptical birefringence of single-mode optical fibers," Appl. Opt. **40**, 5343 (2001).
30. J. Cruz, M. V. Andres, and M. Hernandez, "Faraday effect in standard optical fibers: dispersion of the effective Verdet constant," Appl. Opt. **35**, 922 (1996).
31. K. Zou, J. Wen, Y. Wan, Y. Wu, F. Pang, and T. Wang, "Heat-induced emission enhancement in a Yb:YAG crystal-derived silica fiber," Photonics **9**, 706 (2022).